Nuclear Physics **A460** (1986) 559–580
North-Holland, Amsterdam

THE ^{3}He(α, γ)^{7}Be AND ^{3}H(α, γ)^{7}Li REACTIONS AT ASTROPHYSICAL ENERGIES

Toshitaka KAJINO[1]

Department of Physics, Tokyo Metropolitan University, Fukazawa 2-1-1, Setagaya-ku, Tokyo 158, Japan

Received 16 December 1985
(Revised 3 June 1986)

Abstract: The radiative capture cross sections for ^{3}He(α, γ)^{7}Be and ^{3}H(α, γ)^{7}Li at astrophysical energies have been studied microscopically in terms of the resonating group method. It was found that the astrophysical S-factors correlate strongly to the nuclear size and deformation of ^{7}Be and ^{7}Li. With the help of measured nuclear properties of these nuclei, a safety range of the absolute values of the S-factor was determined; the most recommended $S(0)$-values are 0.50 ± 0.03 keV · b for the ^{3}He(α, γ)^{7}Be reaction and 0.098 ± 0.006 keV · b for the ^{3}H(α, γ)^{7}Li reaction.

1. Introduction

The missing solar neutrino problem is still an unresolved mystery in nuclear astrophysics; the detected number of neutrinos from the sun 2.1 ± 0.3 SNU (1σ error) [1]) is only about a third of the theoretical prediction 5.8 ± 2.2 SNU (3σ error) [2]). The theoretical neutrino flux depends on the rates for the relevant nuclear reactions contributing to the neutrino production in the sun. In the last few decades, much attention has been devoted to measure the absolute cross section for these reactions with less error bar. In spite of much effort, however, the 80–90% of the theoretical uncertainty of the neutrino flux still originates in the uncertainty of the nuclear reaction rates [2]). The rate for ^{3}He(α, γ)^{7}Be is one of these having large experimental discrepancy among several independent observations [3-9]). The most striking discrepancy is found between the two data, $S(0) = 0.30 \pm 0.03$ keV · b [ref. [3])] and $S(0) = 0.52 \pm 0.05$ keV · b [refs. [4,5])] measured respectively by the Münster and Caltech groups, where $S(0)$ being the astrophysical S-factor for the ^{3}He(α, γ)^{7}Be reaction extrapolated to zero energy. According to a standard solar model [2]), theoretical neutrino counting rate in the ^{37}Cl detector is proportional to $S(0)^{0.8}$, and the Caltech $S(0)$ value has been used as a standard one in the theoretical calculation. The measurement of the Münster group, therefore, cast a light that most of the missing solar neutrinos might be accounted for by their small $S(0)$-value. Unfortunately, the discrepancy between the Münster and the Caltech S-factors has not yet been settled experimentally.

[1] Present address: National Superconducting Cyclotron Laboratory, Michigan State University, East Lansing, MI 48824, USA.

Theoretically, Tombrello and Parker [10]) have first succeeded in describing the energy variation of the S-factor very well in a phenomenological direct-capture model. This model needed an overall normalization to fit the calculated values to the observed ones and hence it is not applied to predict the absolute value of the S-factor theoretically. In the extended models by Kim, Izumoto and Nagatani [11]), three $S(0)$-values were obtained without normalization. Although their results were in favor of the Caltech data, they differ from one another depending on the three different phenomenological models adopted. Quite recently, very similar result to Kim *et al.* has been obtained by Buck, Baldock and Rubio [12]). All of these phenomenological models, however, include several ambiguities arising from the potential parameters. In addition, they used approximate dipole operator without taking account of the Pauli principle. These make their calculated S-factors less reliable.

The microscopic cluster model is almost free from these ambiguities. More careful studies of the reaction rate for $^3He(\alpha, \gamma)^7Be$ have been performed by Walliser, Liu, Kanada and Tang [13,14]), the present author [18,19]) and Arima [15]), Hofmann and Mertelmeier [56]), and Langanke [57]) in this microscopic model. These studies are based on the resonating group method. This method has, in fact, provided with a powerful tool for the study of radiative capture reactions of astrophysical interest such as $^{12}C(\alpha, \gamma)^{16}O$ [refs. [16,17])] and $^{16}O(\alpha, \gamma)^{20}Ne$ [ref. [18])] as well as $^3He(\alpha, \gamma)^7Be$ and $^3H(\alpha, \gamma)^7Li$. However, a serious problem remains unresolved in the cluster model calculation that the calculated S-factor depends strongly on the adopted nuclear force. At present we cannot but use effective nuclear force that takes account of a strong α-clustering correlation in light nuclei. But there are many such forces established very well in the microscopic cluster model calculation.

In this article I extended the previous theoretical calculations and found a solution of this problem. Carefully examining the force dependence of the calculated electromagnetic properties of ^7Li and ^7Be as well as the S-factors for $^3H(\alpha, \gamma)^7Li$ and $^3He(\alpha, \gamma)^7Be$, we find a very strong correlation between these observables. We can estimate the possible range of the S-factor by taking account of this correlation with the help of measured nuclear properties of ^7Li and ^7Be. The first aim of this paper is to show the strong correlation among these observables quantitatively. The second and ultimate purpose is to theoretically predict the most feasible absolute $S(0)$ values for $^3He(\alpha, \gamma)^7Be$ and $^3H(\alpha, \gamma)^7Li$.

Although the conjugate mirror reaction $^3H(\alpha, \gamma)^7Li$ has received comparatively little attention, this reaction plays an important role in synthesizing ^7Li in the early universe [20–22]). An only measurement of the cross section by Griffiths *et al.* [23]) has too large error bar, and the S-factor is assumed to be constant $S(0) = 0.065$ keV · b [ref. [24])]. This assumption contradicts clearly to my theoretical calculation showing fairly strong energy variation of the S-factor. An accurate determination of the $S(0)$ value for this reaction also has an important meaning in cosmology. In this article, therefore, the two reactions $^3He(\alpha, \gamma)^7Be$ and $^3H(\alpha, \gamma)^7Li$ are discussed equally.

In the next section, the calculational method is briefly reviewed. In sect. 3, the correlation among the bound state properties of ^{7}Be and ^{7}Li and the S-factors for $^3\mathrm{He}(\alpha, \gamma)^7\mathrm{Be}$ and $^3\mathrm{H}(\alpha, \gamma)^7\mathrm{Li}$ are discussed. The calculated results of the radiative capture cross sections are discussed in sect. 4 in detail. Finally, in sect. 5, the present study is summarized.

2. Method

The single channel resonating group method (RGM) [25]) is adopted in the present study.

In this method the total wave function of the $A = 7$ nuclear systems, ^{7}Li and ^{7}Be, is written as

$$\psi_{(\mathrm{LS})\mathrm{JM}}(\xi_\alpha \xi_\tau \boldsymbol{r}) = \sqrt{\frac{4!3!}{7!}}\, \mathscr{A}_{\alpha\tau}\{[(\phi_\alpha(\xi_\alpha; \beta_\alpha)\phi_\tau^{(S)}(\xi_\tau; \beta_\tau))\otimes\chi_{JL}(r)\, Y^{(L)}(\boldsymbol{r})]_M^{(J)}\}\,. \tag{1}$$

Here $\mathscr{A}_{\alpha\tau}$ is the antisymmetrizer between the nucleons. For the intrinsic wave functions of the constituent nuclei $\phi_i(\xi_i; \beta_i)$, the harmonic oscillator wave functions with different oscillator parameters β_α and β_τ are adopted. The highest spatial symmetries [4] and [3] are assumed for the alpha and triton (or ^{3}He) nuclei, respectively, as in the previous papers [35]). For a given many-body hamiltonian

$$\mathscr{H} = \sum_{i=1}^{7} t_i - T_\mathrm{G} + \sum_{k<l} v_{kl}\,, \tag{2}$$

the intercluster relative wave function $\chi_{JL}(r)$ is determined variationally by solving the RGM equation of motion;

$$\delta\langle\psi_{(LS)JM}(\xi_\alpha\xi_\tau\boldsymbol{r})|\mathscr{H} - E|\psi_{(LS)JM}(\xi_\alpha\xi_\tau\boldsymbol{r})\rangle = 0\,. \tag{3}$$

As the basis vectors for $\chi_{JL}(r)$, the locally peaked gaussian functions [26]) with the width parameter $\nu = \frac{6}{7}\beta_\alpha$ are adopted in order to describe the long distance part of the wave function precisely. The scattering solution of eq. (3) is obtained by using the generalized Kohn-Hulthén-Kato variational principle for the S-matrix [26,27]), and the wave function is normalized to be of unit flux. A spurious c.m. motion is removed exactly by means of Tohsaki's new Generator Coordinate Method [28]) which is applicable to the nuclear systems with different oscillator parameters.

The two-body interaction v_{kl} in the hamiltonian (2) consists of the central and spin-orbit nuclear forces and the Coulomb force. As for the nuclear part we cannot but use effective interaction. In this paper I adopted several different types of the effective interactions in order to see the force dependence of the calculated observables. The central nuclear forces adopted here are classified into the following five types; (i) the Volkov force No. 2 [ref. [29])] (V2), (ii) the modified Hasegawa-Nagata force [30]) (MHN), (iii) the modified Brink-Boeker force No. 1 [ref. [31])] (MBB1), (iv)

the original [32]) and modified [33]) Wildermuth-Tang forces (WT and MWT), and (v) the gaussian forces with single range (G1R) and two ranges (G2R). The former four families are well known and established effective interactions in the microscopic cluster theory based on the G-matrix study: Although they have quite different exchange mixtures, they all give the acceptable binding energy and nuclear size of the α-particle when the shell model configuration [4] $(os)^4$ is assumed. Although there are several modified versions of (i)-(iv), such modifications do not drastically change the calculated results of physical quantities. The last type (v) was constructed phenomenologically by the present author to clarify the discussion in sect. 3. As for the spin-orbit interaction the Nagata force [34]) multiplied by k_{LS} is used, where k_{LS} is the strength parameter. Since the spin-orbit interaction has only a perturbative nature in comparison with the central force, it is not needed to use different interaction.

Only two parameters of the effective interaction are varied; the Majorana mixture parameter m of the central force and the strength parameter k_{LS} of the spin-orbit force. They are adjusted in order to reproduce the cluster separation energy for $^7Li \rightarrow {}^3H + \alpha$ (or $^7Be \rightarrow {}^3He + \alpha$) and the level spacing energy between the ground spin-doublets $\frac{3}{2}^-$ and $\frac{1}{2}^-$. The two parameter values thus determined are shown in tables 1 and 2.

TABLE 1

Parameter values adopted in the present calculation for the $^7Be = {}^3He + \alpha$ system

	V2	MHN	MBB1	WT	MWT	G1R	G2R
Oscillator parameters							
$\beta(\alpha)$ [fm^{-2}]	0.5285	0.574	0.503	0.514	0.604	0.509	0.509
$\beta(^3He)$ [fm^{-2}]	0.393	0.454	0.402	0.367	0.435	0.435	0.435
Majorana-mixture parameter							
m	0.5775	0.3985	0.405	$u = 0.9840$	$u = 0.9840$	0.590	0.502
LS-strength parameter							
k_{LS}	0.55	0.30	0.580	0.280	0.325	0.125	0.368

For the MBB1 (MHN) interaction, the Majorana mixture parameter m of the attractive (intermediate-range attractive) part only is varied as in ref. [35]). Both of the G1R and G2R forces have the Wigner and Majorana exchange mixture parameters as the V2 force. The range and volume parameters are $(\mu_1, v_1) = (2.0\ \text{fm}^{-2}, -337.87\ \text{MeV})$ for the G1R force and $(\mu_i, v_i) = (2.0\ \text{fm}^{-2}, -2810.5\ \text{MeV})$ and $(5.0\ \text{fm}^{-2}, 8797.8\ \text{MeV})$ for the G2R force.

In the same tables the adopted oscillator parameters β_α and β_τ of the constituent clusters are shown, too. These parameter values are determined by fulfilling the variational stability conditions [15,35,36]) for the both clusters α and ^3H (or α and ^3He). These values differ from each other, i.e. $\beta_{^3H} \neq \beta_\alpha$ and $\beta_{^3He} \neq \beta_\alpha$, and give the observed binding energies and charge radii of ^3H, ^3He and α nuclei approximately (fig. 1).

TABLE 2

The same as table 1 for the $^7Li = {}^3H + \alpha$ system

	V2	MHN	MBB1	WT	MWT	G1R	G2R
Oscillator parameters							
$\beta(\alpha)$ [fm^{-2}]	0.5285	0.574	0.503	0.514	0.604	0.509	0.509
$\beta(^3H)$ [fm^{-2}]	0.400	0.460	0.407	0.378	0.440	0.440	0.440
Majorana-mixture parameter m	0.5735	0.39658	0.395	$u = 0.9830$	$u = 0.9830$	0.590	0.495
LS-strength parameter k_{LS}	0.60	0.30	0.580	0.280	0.325	0.125	0.368

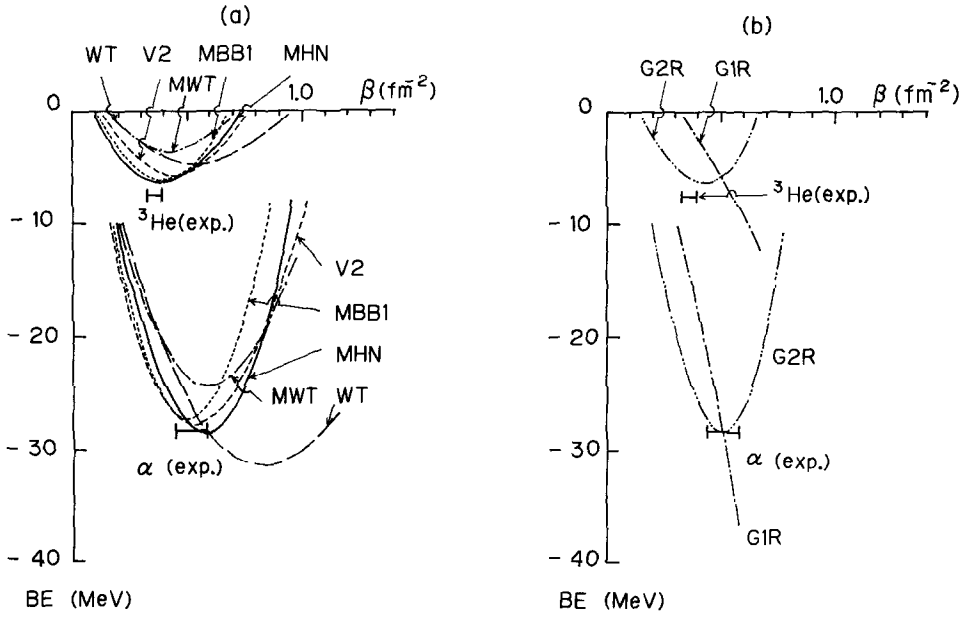

Fig. 1. Binding energy curves $\langle \phi_i(\xi_i; \beta) | h_i | \phi_i(\xi_i; \beta) \rangle$ of the ^{3}He and α-nuclei as functions of β for various effective interactions; (a) for the V2, MHN, MBB1, WT and MWT forces, and (b) for the G1R and G2R forces. Experimental values are from ref. [62]).

Using the microscopic cluster model wave function (1), we calculate the radiative capture cross section in the first order perturbation theory [37]) as

$$\sigma(E_{\mathrm{c.m.}}) = \sum_{\mathrm{E}\lambda,\mathrm{M}\lambda} \frac{8\pi(\lambda+1)}{\lambda\{(2\lambda+1)!!\}^2} \frac{1}{\hbar}\left(\frac{\omega}{c}\right)^{2\lambda+1} \times \frac{1}{2S_i+1} \sum_{J_i,L_i} |\langle (L_f S_f) J_f \| \mathcal{M}^{\mathrm{E(M)}\lambda} \| (L_i S_i) J_i \rangle|^2 , \tag{4}$$

where ω and $E_{\mathrm{c.m.}}$ are the energies of the emitted photon and the incident particle, respectively. $\mathcal{M}^{\mathrm{E(M)}\lambda}$ is the galilean invariant electric (or magnetic) λ-pole operator.

In the present analysis, all available multipole contributions $\lambda \leq 5$ are calculated for the initial partial waves $L_i \leq 3$. Only a contribution of the one-body current is taken into account in the operator $\mathcal{M}^{E(M)\lambda}$. With the use of eq. (4), the astrophysical S-factor is defined [38]) by

$$S(E_{c.m.}) = \sigma(E_{c.m.}) E_{c.m.} \exp(2\pi\eta_c), \tag{5}$$

where $\eta_c = Z_1 Z_2 e^2/\hbar v_i$ is the Sommerfeld parameter, and v_i is the relative velocity between the two incident nuclei. The observed reduced mass is used in eq. (5) for the $^3H+\alpha$ and $^3He+\alpha$ systems, separately. (See subsect. 4.3 for details.)

Details on the practical method are reported in ref. [35]) with several definitions of other important observables, namely the electromagnetic form factors, moments and radii, etc.

3. Correlation between astrophysical S-factor and nuclear size and deformation

3.1. NUCLEAR STRUCTURE OF ^{7}Li AND ^{7}Be

The microscopic cluster model has enjoyed a success for the electromagnetic properties of the light nuclei. The large electric quadrupole moment of ^{7}Li also is explained in this model very well without a serious problem of the spurious c.m. motion [33,35]). However, comparing several theoretical values of this quantity with one another, we soon find the problem that the calculated results somehow depend on an assumed nuclear interaction. In order to determine the reaction rates for $^3H(\alpha, \gamma)^7Li$ and $^3He(\alpha, \gamma)^7Be$ with small error bar, we are led to examine the interaction dependence of the calculated nuclear properties of ^{7}Li very carefully.

In table 3 we summarize the calculated nuclear properties of ^{7}Li. The theoretical values are in a reasonable agreement with the experimental data except one case for the G1R-force. (See subsect. 3.3 for details.) They show a remarkable interaction dependence which correlates strongly to the mean intercluster distance between triron and α. In order to see the correlation clearly we show the intercluster relative wave functions for the MHN and V2 interactions in fig. 2 in comparison with the shell model wave function assuming the [43] $(os)^4(op)^3$ configuration. The clustering component at the nuclear surface region differs from each other depending on the effective interaction and this part makes a large difference of the calculated observables in table 3. The longitudinal Coulomb form factor of ^{7}Li also shows the similar interaction dependence(fig. 3). Though only the two curves for the MHN and V2 interactions are shown in this figure as in fig. 2, the form factors calculated by using the other effective interactions (except for the G1R-force) describe the similar q-dependence between these two curves.

Among a lot of observed electromagnetic properties of ^{7}Li, a particular attention has been paid to determine the electric quadrupole moment in the various measurements [39-44]). A careful comparison between the calculated and measured values of

TABLE 3

Interaction dependence of the calculated S-factors and static electromagnetic properties

	$\sqrt{\langle r_c^2 \rangle}$ [fm]	Q [$e \cdot \mathrm{fm}^2$]	^{7}Li B(E2) [$e^2 \cdot \mathrm{fm}^4$]	$\sqrt{\langle r_M^2 \rangle}$ [fm]	Ω [$\mu_N \cdot \mathrm{fm}^2$]	^{3}He(α, γ)^{7}Be $S(0)$ [keV · b]	^{3}H(α, γ)^{7}Li $S(0)$ [keV · b]
exp.							
	2.39 ± 0.03 [a]	−3.70 ± 0.08 [d]	8.3 ± 0.5 [d]	2.98 ± 0.05 [b]	|9.3 ± 0.4| [b]	0.30 ± 0.03 [k]	0.100 ± 0.025 [r,s]
	2.55 ± 0.07 [b]	−3.43 ± 0.02 [e]	7.42 ± 0.14 [i]			0.47 ± 0.05 [l]	
	2.35 ± 0.10 [c]	−3.66 ± 0.03 [f]	8.3 ± 0.6 [j]			0.61 ± 0.07 [m]	
		−4.1 ± 0.6 [g]				0.53 ± 0.03 [n]	
		−3.7 ± 0.3 [h]				0.63 ± 0.04 [o]	
		−4.0 ± 1.1 [i]				0.56 ± 0.03 [p]	
						0.47 ± 0.04 [q]	
cal.							
V2	2.55	−4.41	10.57	3.04	−10.45	0.841	0.174
MHN	2.35	−3.50	6.61	2.81	−8.71	0.500	0.098
MBB1	2.56	−4.38	10.27	3.05	−10.57	0.694	0.141
WT	2.44	−3.70	7.55	-	-	0.698 [t]	0.146
MWT	2.39	−3.73	7.46	-	-	0.609†	0.120
G1R	2.15	−2.13	2.46	2.57	−6.56	0.312	0.0631
G2R	2.43	−3.71	7.40	2.89	−9.41	0.488	0.0969

† This value is a little different from $S(0) = 0.598$ keV · b in ref. [14]) because the variational stability conditions [35]) are satisfied in the present calculation.

[a]) Ref. [58]) [b]) Ref. [59]) [c]) Ref. [60]) [d])-[i]) Refs. [39-44]) [j]) Ref. [61])
[k])-[q]) Refs. [3-9]) [r]) Ref. [20]) [s]) Ref. [23]) [t]) Ref. [13])

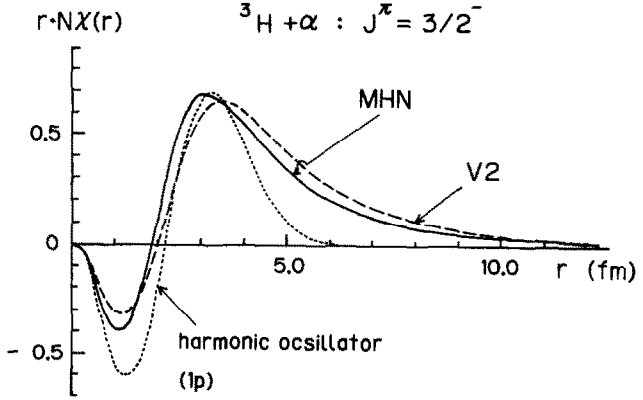

Fig. 2. $^3H+\alpha$ reduced width amplitudes of the ground state of ^7Li. Solid and dashed curves are the calculated results by using the MHN and V2 interactions, respectively. Dotted curve represents the harmonic oscillator function $r \cdot u_{1p}(r; \nu)$ with $\nu = \frac{12}{7} \times 0.32\ \mathrm{fm}^{-2}$.

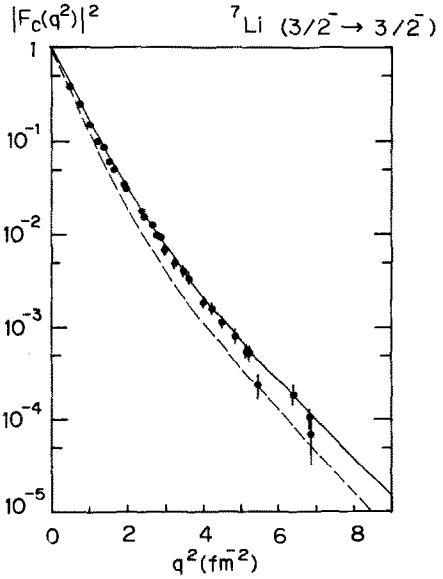

Fig. 3. Squared longitudinal Coulomb form factors of ^7Li. Solid and dashed curves are the same as those in fig. 2. Black disks are the data of ref. [58]).

this quantity is a very crucial test of the assumed effective interaction. From table 3 and fig. 5(b), we can conclude that the MHN interaction is the most desirable effective interaction in order to describe the electromagnetic structure of ^7Li.

There are few data on the structure of ^7Be because this nucleus is unstable. Only the $B(M1)$ strength for the transition between the ground spin-doublets has been measured; 1.92 ± 0.25 [ref. [45])] and 2.7 ± 1.0 [ref. [46])] in unit of μ_N^2, where μ_N is the nuclear magneton. Although the experimental error bar is large, the microscopic

^{3}He+α cluster wave function gives a reasonable value 1.59 μ_N^2 with the use of the MHN interaction.

3.2. ^{3}He+α AND ^{3}H+α SCATTERINGS

The calculated nuclear phase shifts for the elastic scatterings ^{3}He(α, α)^{3}He and ^{3}H(α, α)^{3}H are compared with observations [47]) in figs. 4a and b. Although present model gives substantially a good approximation to the low energy scatterings, only the f-wave ($f_{7/2}$ and $f_{5/2}$) phase shifts are not satisfactory near the resonance energies. This is a well known anomaly [32]) as regards the spin-orbit and tensor interactions in the $A=7$ nuclear systems, which has not been solved quantitatively in any microscopic model. Fortunately, however, the two reactions ^{3}He(α, γ)^{7}Be and ^{3}H(α, γ)^{7}Li are almost free from the anomaly because the s-wave contribution predominates at the low energies. In fact, the f-wave contribution is negligibly small at astrophysical energies $E_{c.m.} = 1$–20 keV, and only 1% at $E_{c.m.} \approx 2$ MeV. (See sect. 4 for details.)

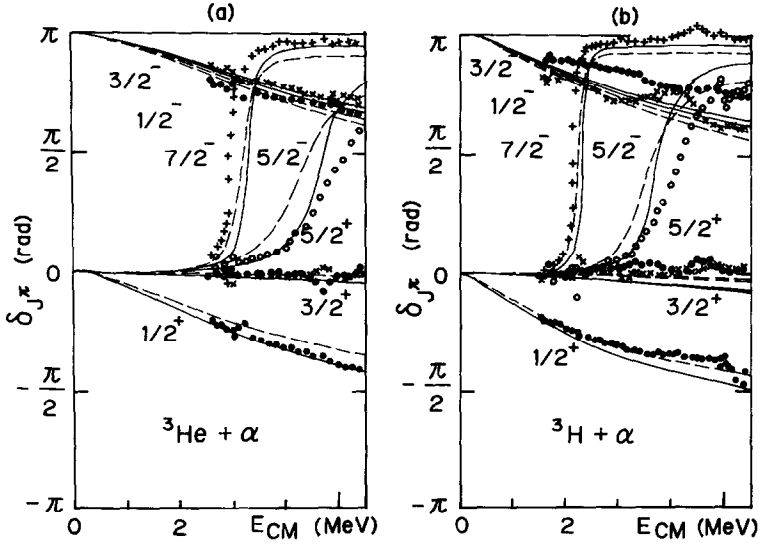

Fig. 4. Nuclear phase shifts for the elastic scatterings; (a) for the ^{3}He(α, α)^{3}He scattering, and (b) for the ^{3}H(α, α)^{3}H scattering. Solid and dashed curves are the same as those in fig. 2. Crosses and dots are the data of experimental phase shifts analysis of ref. [47]).

The observed nuclear phase shifts for positive parity channels show a typical behavior of the hard core scattering. The present calculation describes it very well. In the microscopic cluster model the intercluster relative wave function with $L=0$ (or 1 and 2) has two (or one) energy independent radial nodes by the requirement of the Pauli exclusion principle, and the outermost node among them plays the

same role as the phenomenological hard core radius. Since the hard core radius affects the low energy reaction very much as is known in the effective range theory, Tombrello and Parker [10]) adopted the core radius 2.8 fm for the s- and d-waves in a phenomenological way in order to reproduce the observed phase shifts. This value is in a reasonable agreement with 2.5 fm which is the position of the outermost node indicated in the present microscopic calculation.

It should be noted that the interaction dependence of the scattering wave function is very weak at the energies far below the Coulomb barrier in contrast with the bound state wave function: Whatever effective interaction we may use, the radial shape of the relative wave function is similar within the difference of ±3% for $E_{c.m.} \leqslant 200$ keV. The reason is clear: At such astrophysical energies, the tail of the Coulomb barrier makes it difficult to find two charged nuclei ^{3}He and α or ^{3}H and α in close distance from each other. The nuclear interaction, therefore, does not affect the intercluster relative wave function.

3.3. CONSTRAINT ON THE UPPER AND LOWER BOUNDS OF ASTROPHYSICAL S-FACTOR

Table 3 shows both of the experimental and theoretical S-factors and the static nuclear properties of ^{7}Li. Every observable in this table has a dimension depending on the length and show a similar interaction dependence. As was discussed in the last two subsections, the bound state wave function is influenced very much by the nuclear interaction, while the scattering wave function at the low energy is not. This is the reason why the S-factor, though this is the dynamical property, has a remarkable interaction dependence similar to the static nuclear properties.

It is worth noting here that there is a strong and approximately linear correlation between these properties. In order to see it more clearly the two sets of the observables $(\sqrt{\langle r_c^2 \rangle}, S(0))$ and $(Q, S(0))$ are plotted in figs. 5a and b, where $S(0)$ is the S-factor for ^{3}He$(\alpha, \gamma)^7$Be. Almost the same correlation is found, of course, between the static properties and $S(0)$ value for ^{3}H$(\alpha, \gamma)^7$Li. As shown in these figures, the nuclear size and deformation of the final bound state gives a strong constraint on the absolute $S(0)$ value. Using the correlation, we can quantitatively estimate the absolute $S(0)$ value which is consistent with the observed nuclear properties of ^{7}Li;

$$0.4 \text{ keV} \cdot \text{b} \leqslant S(0) \leqslant 0.9 \text{ keV} \cdot \text{b}$$

for the ^{3}He$(\alpha, \gamma)^7$Be reaction and

$$0.08 \text{ keV} \cdot \text{b} \leqslant S(0) \leqslant 0.19 \text{ keV} \cdot \text{b}\,, \tag{6}$$

for the ^{3}H$(\alpha, \gamma)^7$Li reaction. Although there are many different theoretical $S(0)$ values [11-15]) for ^{3}He$(\alpha, \gamma)^7$Be which were calculated in the various models without normalization, they all are in the range estimated above. The energy variation of the S-factor is shown for the typical effective interactions in figs. 6a and b. All

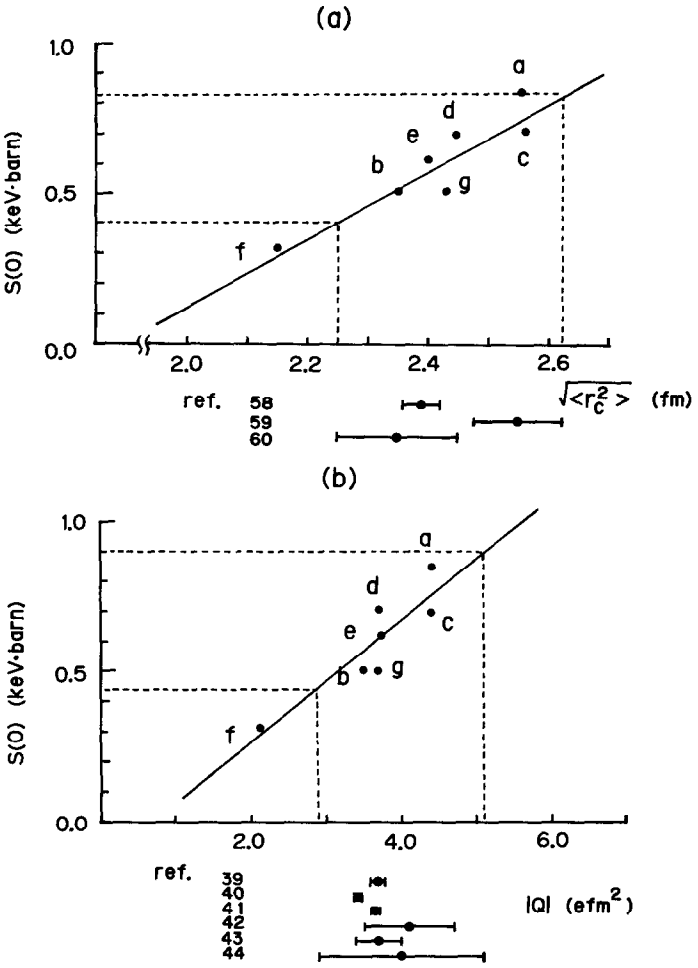

Fig. 5. Correlation between the S-factor for $^3He(\alpha, \gamma)^7Be$ and the charge radius (a) and the electric quadrupole moment (b) of ^7Li. In each graph, a, b, c, d, e, f and g denote the calculated results by using the V2, MHN, MBB1, WT, MWT, G1R and G2R interactions, respectively. Solid lines represent the approximately linear correlation between these quantities which were obtained by χ^2 fitting to the calculated values. Experimental values are from refs. [58-60]) for $\sqrt{\langle r_c^2 \rangle}$ in (a), and refs. [39-44]) for Q in (b).

curves describe very similar energy variation although the absolute values differ from one another. The theoretical curve using the MHN interaction among them explains the Caltech data [4-6]) for $^3He(\alpha, \gamma)^7Be$ and the Griffith's data [23]) for $^3H(\alpha, \gamma)^7Li$ quite systematically. Note here again that the MHN interaction gives the best description of the nuclear structure in particular the electric quadrupole moment of ^7Li among many established effective interactions. As for the discrepancy of the S-factor for $^3He(\alpha, \gamma)^7Be$, the Caltech data are reliable more than the Münster ones [3]) from the theoretical viewpoint.

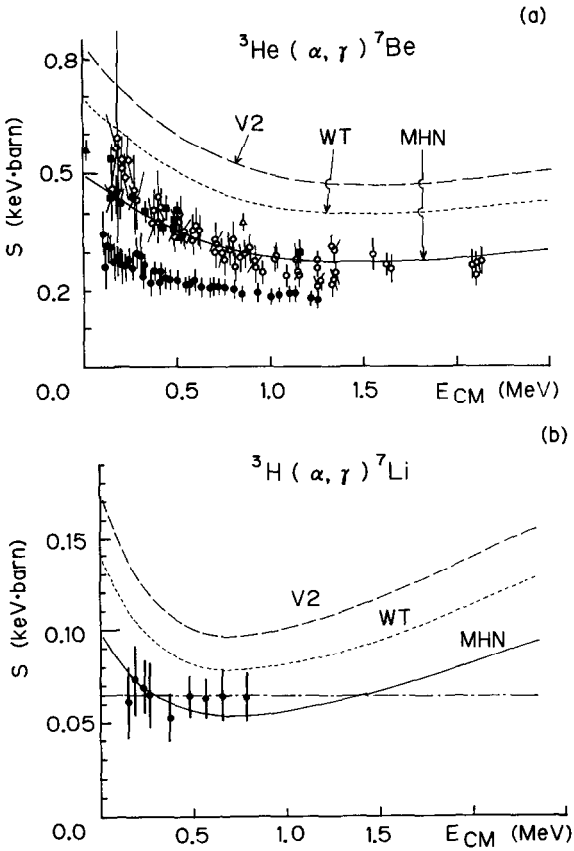

Fig. 6. Energy variation of the S-factor; (a) for the $^3He(\alpha, \gamma)^7Be$ reaction, and (b) for the $^3H(\alpha, \gamma)^7Li$ reaction. Solid, dashed and dotted curves are the calculated results by using the typical effective interactions, the MHN, V2 and WT forces, respectively. Dot-dashed line in (b) denotes $S(0) = 0.065$ keV · b which has been assumed in the big-bang nucleosynthesis calculation [24]). (See sects. 1 and 4.2.) See text and table 3 on the calculated results by using the other effective interactions. The experimental data are from ref. [3]) (●), ref. [4]) (○), ref. [5]) (◇), ref. [6]) (■), ref, [7]) (△), ref. [8]) (▲) and ref. [9]) (★) for the $^3He(\alpha, \gamma)^7Be$ reaction and from ref. [23]) (●) for the $^3H(\alpha, \gamma)^7Li$ reaction.

The present author examined carefully whether it is possible or not to make a phenomenological interaction so that the small values of the Münster S-factor are well explained. The result was that it is very difficult to construct such a force for two reasons. First, we cannot explain the static nuclear properties consistently with the small S-factor like Münster's: As an example the phenomenological G1R force was constructed in order to reproduce the Münster S-factor. The folding potential between the two clusters α and ^3H with this force vanishes rapidly as the intercluster distance increases as displayed in fig. 7. As the result, the intercluster relative wave function of ^7Li shrinks very much and the charge radius, the quadrupole moment, etc. become too small in comparison with observations. (See figs. 7a and b.)

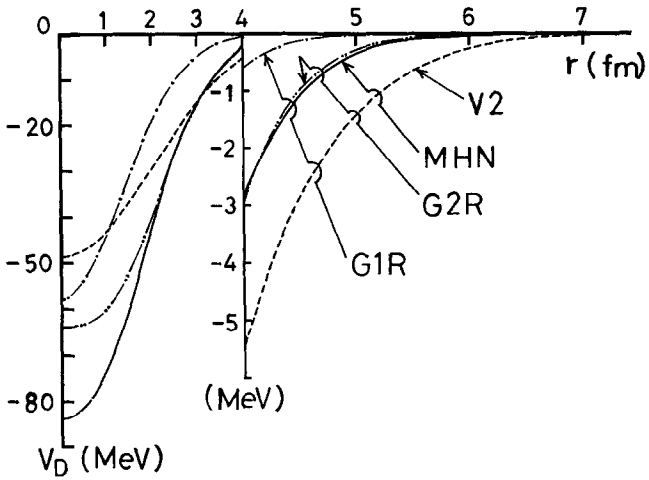

Fig. 7. Direct folding nuclear potentials between ^3H and α for the typical effective interactions (the MHN, V2, G1R and G2R forces).

Second, one encounters another serious problem with the G1R-force: The attractive range of this interaction is so short that the variational stability conditions are not at all satisfied for the constituent nuclei ^3He, ^3H and α. (Compare fig. 1b with fig. 1a.) To restore the conditions I introduced a repulsive soft-core, and the two strength parameters for the attractive and repulsive parts were determined to reproduce the observed binding energy and charge radius of alpha nucleus. The range of the repulsive part is set equal to that of the soft core potential proposed by Tamagaki [48]). The gaussian force with two ranges (G2R-force) thus constructed gives the folding potential which is very similar to that given by the MHN interaction (fig. 7). The intercluster relative wave function and the S-factor also become very close to those calculated with the MHN interaction. The electromagnetic properties of ^7Li are again in reasonable agreement with observations (table 3).

I repeated the same procedure as the present analysis for various values of the two range-parameters in the gaussian potentials. Quite the similar results were obtained for all of them. Whenever one adds a soft-core to the phenomenological interaction in order to satisfy the stability conditions for the constituent nuclei, the calculated astrophysical S-factor becomes nearly equal to or larger than the Caltech data for the $^3He(\alpha, \gamma)^7Be$ reaction.

4. Discussions

Several calculated observables for the $^3He(\alpha, \gamma)^7Be$ and $^3H(\alpha, \gamma)^7Li$ reactions are compared with observations in this section. In the theoretical calculation the modified Hasegawa-Nagata force was used as an effective interaction.

4.1. $^3He(\alpha, \gamma)^7Be$ REACTION

The electric dipole (E1) transition predominates in many possible multiple contributions. The sum of the higher multipoles (E2, E3 - - - and M1, M2 - - -) is only less than 1% of the total cross section for $E_{c.m.} \leq 2$ MeV. Decomposition of the E1 cross section into partial wave contributions ($s_{1/2}$, $d_{5/2}$ and $d_{3/2}$) manifests that the d-wave has an appreciable strength even at the low energies of astrophysical interest; this contribution amounts to 10% or so at $E_{c.m.} = 500$ keV (figs. 8a and b). It is worth noting that the significantly large d-wave contribution has been found in another nuclear reaction $^7Be(p, \gamma)^8B$ by Barker and Spear [49]), which affects more or less the theoretical neutrino counting rate. There is an $f_{7/2}$ resonance at $E_{c.m.} \doteqdot 2.98$ MeV which is the lowest resonance of ^7Be in the $^3He + \alpha$ continuum. Possible multipoles as regards the resonance are E2, E4, M3 - - - (or E4, M3 - - -) for the transition leading to the ground (or the first excited) state. Although these multipole cross sections are increased around the resonance energy, an off-resonance behavior at the lower energy region is not modified strongly. (See the energy dependence of the $f_{7/2}$ contribution in fig. 8a.)

The calculated branching ratio is compared with the experimental data in fig. 9a. It was found in the previous paper [15]) that the absolute value about 0.4 is explained by the two contributions, i.e. the photon phase space factor and the nuclear matrix element. More detailed study discloses that the two factors have quite different

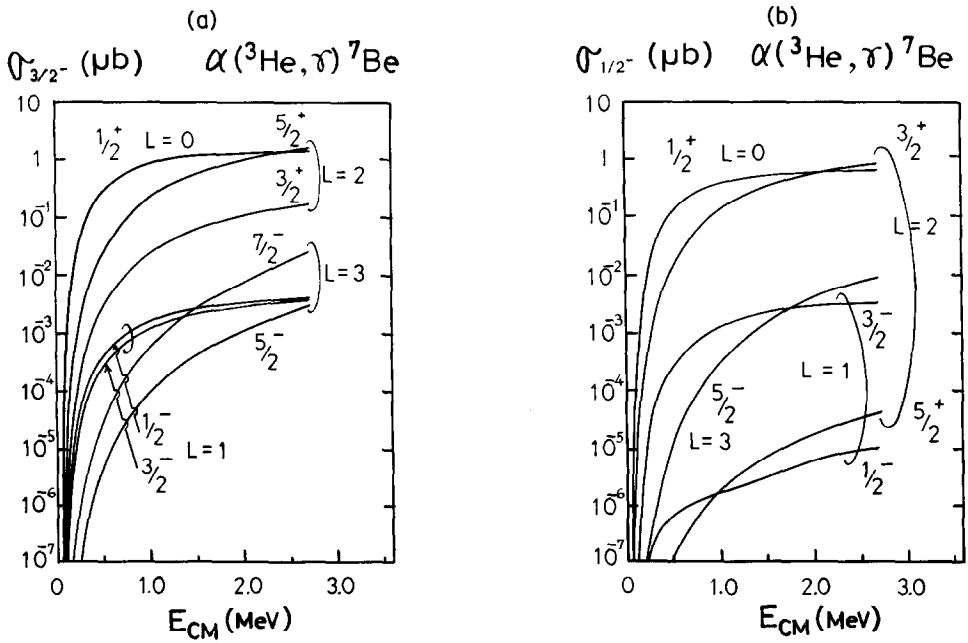

Fig. 8. Decomposition of the calculated cross sections for the $^3He(\alpha, \gamma)^7Be$ reaction into partial wave contributions; (a) and (b) are for the transitions leading to the ground ($\frac{3}{2}^-$) and first excited ($\frac{1}{2}^-$) states.

energy dependence from each other and a very weak energy dependence of the branching ratio results from a counterbalance of these two factors. This is demonstrated in fig. 9(a) for the predominant E1 transition. The photon phase space factor $[(2J_f+1)\omega^{2\lambda+1}]_{J_f^\pi=1/2^-}/[(2J_f+1)\omega^{2\lambda+1}]_{J_f^\pi=3/2^-}$ varies as 0.2–0.33 for $E_{c.m.}=$ 10–2500 keV due to the different binding energies of the ground and first excited states. (Note that $\hbar\omega = E_{c.m.} + \mathrm{BE}(J_f^\pi)$, where $\mathrm{BE}(J_f^\pi)$ is the binding energy of the state $J_f^\pi = \frac{3}{2}^-$ or $\frac{1}{2}^-$ measured from the cluster separation threshold.) On the other hand, the nuclear matrix element factor $|\langle\frac{1}{2}^-\|\mathcal{M}^{(E1)}\|J_i^+\rangle|^2/|\langle\frac{3}{2}^-\|\mathcal{M}^{(E1)}\|J_i^+\rangle|^2$ makes a decreasing energy dependence as 2.0–1.2 with increasing energy $E_{c.m.}=$ 10–2500 keV. Multiplying (0.2–0.33) by (2.0–1.2), we obtain the almost energy independent value 0.4 for all over the energy region $0 \lesssim E_{c.m.} \lesssim 2.5$ MeV.

The thermonuclear reactions are presumed to proceed at very low energies $E_{c.m.} = 1$–20 keV under the prevailing condition $T_{eff} \doteqdot 10^7$ K at the center of the sun. It therefore is relevant to extract the astrophysical S-factor at absolute zero energy from the theoretical calculation. By means of eqs. (6) in ref. [20]) we extrapolated the calculated S-factor at $E_{c.m.} \geqslant 10$ keV to zero energy. The result is

$$S(0) = 0.50 \pm 0.03 \text{ keV} \cdot \text{b}\,, \tag{7a}$$

$$\frac{1}{S(0)}\frac{\partial S(0)}{\partial E_{c.m.}} = -0.548 \pm 0.033 \text{ MeV}^{-1}\,, \tag{7b}$$

for the $^3\mathrm{He}(\alpha, \gamma)^7\mathrm{Be}$ reaction. The theoretical error bar is ±6% which will be discussed in subsect. 4.3. The logarithmic derivative is in a reasonable agreement with the previous calculation of Williams and Koonin [50]). The absolute $S(0)$ value is compared with available data in table 3. The present result is consistent with the Caltech data [4,5]) and several new measurements of Osborne *et al.* [6]), Robertson *et al.* [7]) and Alexander *et al.* [9]).

4.2. $^3\mathrm{H}(\alpha, \gamma)^7\mathrm{Li}$ REACTION

The mirror reaction $^3\mathrm{H}(\alpha, \gamma)^7\mathrm{Li}$ manifests several similarities to $^3\mathrm{He}(\alpha, \gamma)^7\mathrm{Be}$; the branching ratio (figs. 9a and b), the multipole and partial wave contributions (fig. 10 and fig. 2 of ref. [15]), etc. show generally an analogous behavior very much. Quantitatively, however, there are many interesting differences from each other.

The most significant difference is the energy dependence of the S-factor at very low energies which is concerned with the big-bang nucleosynthesis of ^{7}Li [ref. [20])] (figs. 6a and b). In order to see the difference quantitatively, $S(0)$ value for the $^3\mathrm{H}(\alpha, \gamma)^7\mathrm{Li}$ reaction and its logarithmic derivative were calculated in the same way as $^3\mathrm{He}(\alpha, \gamma)^7\mathrm{Be}$;

$$S(0) = 0.098 \pm 0.006 \text{ keV} \cdot \text{b}\,, \tag{8a}$$

$$\frac{1}{S(0)}\frac{\partial S(0)}{\partial E_{c.m.}} = -2.056 \pm 0.123 \text{ MeV}^{-1}\,, \tag{8b}$$

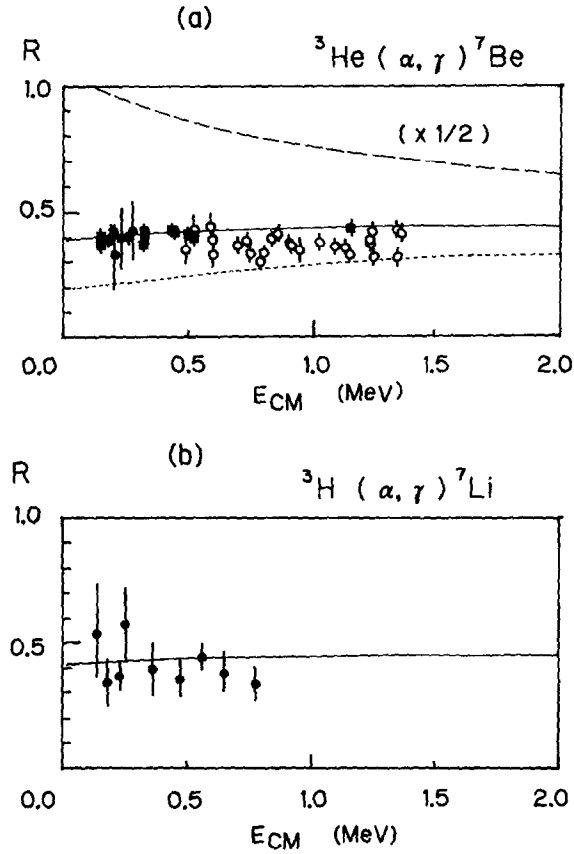

Fig. 9. Calculated branching ratios (solid curves) for the $^3He(\alpha, \gamma)^7Be$ (a) and $^3H(\alpha, \gamma)^7Li$ (b) reactions in comparison with observations. The experimental data are from ref. [4]) (○), ref. [5]) (●) and ref. [6]) (■) for the $^3He(\alpha, \gamma)^7Be$ reaction and ref. [23]) (●) for the $^3H(\alpha, \gamma)^7Li$ reaction. Dashed and dotted curves are the contributions of the reduced E1 matrix element and the photon phase space factors, respectively. (See text.)

which should be compared with (7a) and (7b). About four times stronger energy variation of S is predicted for $^3H(\alpha, \gamma)^7Li$ than $^3He(\alpha, \gamma)^7Be$ in the present calculation. The S-factor for $^3H(\alpha, \gamma)^7Li$ increases very strongly as the incident energy becomes lower than 0.5 MeV as displayed in fig. 6b. As the result, the absolute $S(0)$ value is expected to be 50% larger than $S(0) = 0.065$ keV · b which is the value adopted in the big-bang calculation [24]). In addition, the S-factor has been assumed to be constant previously. Williams and Koonin [50]) have also predicted as large logarithmic derivative for $^3H(\alpha, \gamma)^7Li$ as the present result. However, the large error bar of the experimental data [23]) masks such a strong energy variation of S. An independent measurement is highly required.

Another interesting difference was found [15]) in the absolute cross section and S-factor between the two reactions. This difference was explained theoretically as

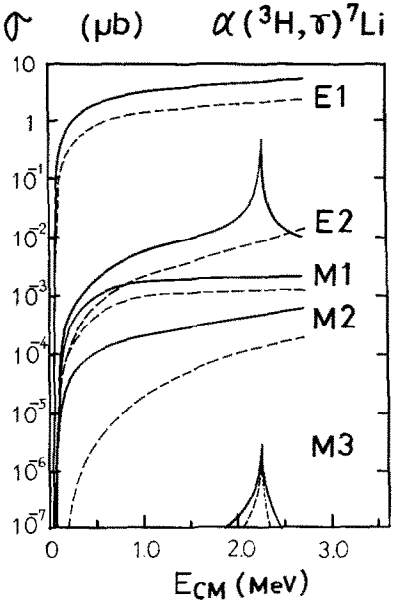

Fig. 10. Decomposition of the calculated cross sections for the $^3H(\alpha, \gamma)^7Li$ reaction into multipolarities. Solid and dashed curves represent two contributions from the transitions leading to the ground ($\frac{3}{2}^-$) and first excited ($\frac{1}{2}^-$) states of ^7Li, respectively.

the result of the different threshold effect which controls sensitively the mean intercluster distance between triton and α or ^3He and α in conjunction with the different role of the isovector part in the electromagnetic interaction. It is to be noted that the same microscopic cluster model calculation [35]) predicts many differences of the nuclear structure between ^7Li and ^7Be, too.

Finally in this subsection, I would like to comment on the resonance effect. In the continuum of ^7Li there is a $f_{7/2}$ resonance at $E_{c.m.} \doteqdot 2.2$ MeV just as in the ^7Be nucleus. The contributing multipole cross sections show narrow peak, corresponding to an α-decay width of $\Gamma_\alpha = 93 \pm 8$ keV (fig. 10). It is to be stressed that this low-lying resonance does not affect much the total cross section at the lower energies.

4.3. ESTIMATE OF THE THEORETICAL ERROR

We have at least two sources of the theoretical error which is attached to the calculated S-factor.

The first one is the uncertainty in the tail part of the constructed wave function. At the low energies far below the Coulomb barrier, an incident ^3He or triton nucleus is captured by an alpha-particle in the external region 5 fm $\lesssim r \lesssim$ 25 fm. An accuracy of the calculated cross section, therefore, depends strongly on the accuracy of the wave function in this region. The tail part of the bound state wave function, which was constructed very carefully up to $r = 35$ fm, is entirely very close to the Whittacker

function [51]) as displayed in fig. 11. Although the scattering wave function has a very small amplitude as shown in the same figure, unitarity of the S-matrix is satisfied with sufficiently high precision as $|S| = 1 \pm 10^{-7}$ for $E_{\mathrm{c.m.}} \geq 10$ keV*. Using these wave functions, we here examine the contribution of the long distance component of the wave function to the predominant E1 matrix element. For this purpose we take a local approximation as

$$\langle L_f \| \mathcal{M}^{(\mathrm{E1})} \| L_i \rangle \simeq \lim_{R_0 \to -\infty} \int_0^{R_0} \sqrt{N}\, \chi_{J_f L_f}(r) \mathcal{M}_{\mathrm{D}}^{(\mathrm{E1})}(r) \sqrt{N}\, \chi_{J_i L_i}(r) r^2 \, \mathrm{d}r, \tag{9}$$

where N is the normalization kernel and $\mathcal{M}_{\mathrm{D}}^{(\mathrm{E1})}(r)$ is the direct part of the E1 operator acting on the intercluster relative coordinate r;

$$\mathcal{M}_{\mathrm{D}}^{(\mathrm{E1})}(r) = C_{J_i^\pi} \frac{A_1 A_2}{A_1 + A_2} \left(\frac{Z_1}{A_1} - \frac{Z_2}{A_2} \right) r,$$

$$C_{J_i^\pi} = \begin{cases} \sqrt{3/4\pi}\,, & \text{for } J_i^\pi = \frac{1}{2}^+, \\ \sqrt{6/4\pi}\,, & \text{for } J_i^\pi = \frac{5}{2}^+ \text{ and } \frac{3}{2}^+. \end{cases} \tag{10}$$

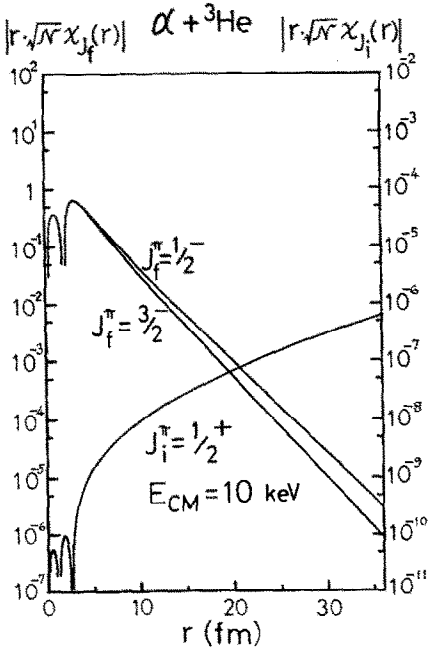

Fig. 11. Calculated intercluster relative wave functions of the scattering state with $J_i^\pi = \frac{1}{2}^+$ at $E_{\mathrm{c.m.}} = 10$ keV and the bound states with $J_f^\pi = \frac{3}{2}^-$ and $\frac{1}{2}^-$ for the $^3\mathrm{He} + \alpha$ system. Note that the measures for the scattering and bound state wave functions differ from each other.

* An accuracy of the Coulomb functions holds the key to constructing the precise scattering wave function. Our Coulomb functions have quite the same accuracy as Barnett's ones [52]) even at the low energy 6.86 keV.

This approximation is more reliable as the incident energy becomes lower. In practice, this gives a very close value to the correct matrix element obtained in the full RGM calculation with a very small error less than 0.01% for $E_{c.m.} \leqslant 100$ keV. Fig. 12 shows the matrix element (9) as a function of R_0, the upper bounds of the integral regarding r, at $E_{c.m.} = 10$ keV which is the lowest energy in the present calculation. An excellent convergence is achieved for $R_0 \geqslant 30$ fm. Based on this calculation, we estimate that the present RGM calculation has an error less than $\pm 3\%$.

The second error bar arises from the choice of the reduced mass for the $^3He + \alpha$ or $^3H + \alpha$ system. In the framework of the non-relativistic quantum many-body theory, one cannot but ignore the proton-neutron mass difference for the sake of removing the c.m. motion and for the practical reason. The best choice is to use the reduced mass $\mu = \frac{12}{7} \times M_N$ with $M_N = 931.452$ MeV for the $^3He(\alpha, \gamma)^7Be$ reaction and $M_N = 931.307$ MeV for the $^3H(\alpha, \gamma)^7Li$ reaction so that the above theoretical values of μ reproduce the observed ones μ(exp.), as was discussed in ref. [14]). With this choice of μ one can describe the asymptotic behavior of the intercluster relative wave function correctly. By setting $\mu = \mu$(exp.), we obtained the value $S(10\text{ keV}) = 0.496$ keV · b for the $^3He(\alpha, \gamma)^7Be$ reaction. Another choice $\mu = \frac{12}{7} \times M'_N$ with $M'_N = (M_p + M_n)/2 = 938.905$ MeV also is usually used in the resonating group calculation, where M_p and M_n are the proton and neutron masses, respectively. $S(10\text{ keV}) = 0.508$ keV · b was obtained [15]) in the latter case. Although both choices of μ are

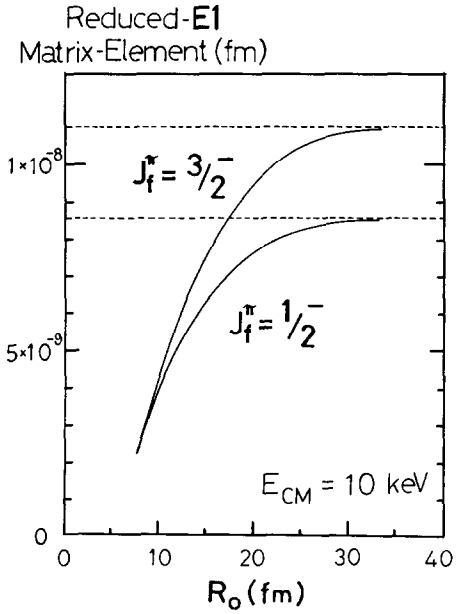

Fig. 12. Saturation behaviors of the reduced E1 matrix elements for the $^3He(\alpha, \gamma)^7Be$ reaction at $E_{c.m.} = 10$ keV as functions of the upper limit R_0 of the integral regarding r. (See text.)

approximations ignoring the proton–neutron mass difference, the calculated S-values are in good agreement with each other within the error bar ±2.5%.

Taking account of the two independent errors ±3% and ±2.5%, we estimate the total theoretical error bar to be at most ±6%.

5. Summary

Two radiative capture reactions $^3He(\alpha, \gamma)^7Be$ and $^3H(\alpha, \gamma)^7Li$ have been studied from the microscopic viewpoint in this paper. It was found that the calculated S-factors for the two reactions and the static nuclear properties of ^7Be and ^7Li correlate strongly to each other. Using this correlation with the help of measured nuclear properties of ^7Li, we determined the possible range of the S-factors; $0.4\,\text{keV}\cdot\text{b} \leqslant S(0) \leqslant 0.9\,\text{keV}\cdot\text{b}$ for $^3He(\alpha, \gamma)^7Be$ and $0.08\,\text{keV}\cdot\text{b} \leqslant S(0) \leqslant 0.19\,\text{keV}\cdot\text{b}$ for $^3H(\alpha, \gamma)^7Li$. As the result, one can conclude that the S-factors for $^3He(\alpha, \gamma)^7Be$ measured by the Caltech groups and the recent reexamined ones are consistent with those for $^3H(\alpha, \gamma)^7Li$ measured by Griffiths *et al.*

For the $^3He(\alpha, \gamma)^7Be$ reaction, the most recommended theoretical $S(0)$ value is $S(0) = 0.50 \pm 0.03\,\text{keV}\cdot\text{b}$. This value is very close to $0.52 \pm 0.05\,\text{keV}\cdot\text{b}$ which has been adopted in predicting the solar neutrino counting rate in the ^{37}Cl detector. Although only a small modification of the solar neutrino flux [20]) is made by the use of the present $S(0)$ value instead of the previous one, it was clarified in this paper that the uncertainty of the nuclear reaction rate for $^3He(\alpha, \gamma)^7Be$ is not responsible for the missing solar neutrino problem.

As for the $^3H(\alpha, \gamma)^7Li$ reaction, $S(0) = 0.098 \pm 0.006\,\text{keV}\cdot\text{b}$ is recommended in the present study. Both of the absolute values and the energy dependence of the S-factor are different from the previous empirical estimate [24]) very much. This leads to a prediction that the nuclear reaction rate $\langle\sigma v\rangle$ becomes 20%–40% larger than the previous calculation for the relevant energy region $T \leqslant 10^9$ K of cosmological interest. The calculated result of primordial ^7Li abundance in the big bang model is reported elsewhere [20]).

In the present analysis, the following conditions are satisfied exactly in order to remove theoretical uncertainties from the calculated S-factor; the variational stability conditions for the constituent clusters, the removal of the spurious c.m. motion, the conservation of the electric dipole current, the exact treatment of the Pauli principle, and so on. Several authors [17]) also confirm the significance of the Pauli principle in another system. However, the following three effects have not been considered here; the meson exchange currents, the d-state mixing in the constituent nuclei ^3H, ^3He and ^4He and the coupling with inelastic channels. The meson exchange currents do not contribute largely to the radiative capture cross sections for $^3He(\alpha, \gamma)^7Be$ and $^3H(\alpha, \gamma)^7Li$ because of the E1-dominance of these reactions. In the present calculation the electric dipole (E1) current is conserved owing to the Siegert theorem [53]) without taking account of the two-body currents such as the meson

exchange currents. The effect of the d-state mixing and the symmetry breaking effect may slightly reduce the calculated S-factor. However, such a reduction is expected to be a few percent because an admixture of the lower symmetry states such as the [421] symmetry is at most 3% according to the intermediate-coupling shell model calculations by Barker [54]) and Cohen and Kurath [55]). It has been reported [56]) quite recently that the inelastic channel such as $^7Be \rightarrow {}^6Li + p$ does not strongly influence the astrophysical S-factor for $^3He(\alpha, \gamma)^7Be$ at very low energies, although it affects more or less the higher energy region. At present, therefore, we cannot find any reason that modifies the present result of the S-factors very much.

The author wishes to express his deep appreciation to A. Arima, K.-I. Kubo, H. Toki, K. Yazaki and S. Austin for many helpful discussions and comments. The numerical calculations of this work have been performed by using M-280H at the Computer Center, University of Tokyo and financially supported by the Institute for Nuclear Study, University of Tokyo and the Research Center for Nuclear Physics, Osaka University.

References

1) R. Davis, Jr., D.S. Harmer and K.C. Hoffman, Phys. Rev. Lett. **20** (1968) 1205;
R. Davis, Jr., Bull. Am. Phys. Soc. **29** (1984) 731
2) J.N. Bahcall *et al.*, Rev. Mod. Phys. **54** (1982) 767; Astrophys. J. **292** (1985) L79
3) H. Kräwinkel *et al.*, Z. Phys. **A304** (1982) 307
4) P.D. Parker and R.W. Kavanagh, Phys. Rev. **131** (1963) 2578
5) K. Nagatani, M.R. Dwarakanath and S. Ashery, Nucl. Phys. **A128** (1969) 325
6) J.L. Osborne *et al.*, Phys. Rev. Lett. **48** (1982) 1664; Nucl. Phys. **A419** (1984) 115
7) R.G.H. Robertson *et al.*, Phys. Rev. **C27** (1983) 11
8) H. Volk *et al.*, Z. Phys. **A310** (1983) 91
9) T.K. Alexander *et al.*, Nucl. Phys. **A427** (1984) 526
10) T.A. Tombrello and P.D. Parker, Phys. Rev. **131** (1963) 2582
11) B.T. Kim, T. Izumoto and K. Nagatani, Phys. Rev. **C23** (1981) 33
12) B. Buck, R.A. Baldock and J.A. Rubio, J. of Phys. **G11** (1985) 611
13) H. Walliser *et al.*, Phys. Rev. **C28** (1983) 57
14) H. Walliser, H. Kanada and Y.C. Tang, Nucl. Phys. **A419** (1984) 133
15) T. Kajino and A. Arima, Phys. Rev. Lett. **52** (1984) 739
16) K. Langanke and S. Koonin, Nucl. Phys. **A439** (1985) 384
17) P. Descouvemont, D. Baye and P.-H. Heenen, Nucl. Phys. **A430** (1984) 426;
D. Baye and P. Descouvemont, Nucl. Phys. **A410** (1983) 334
18) T. Kajino, Lecture Notes in Physics **219** (1985) 85
19) T. Kajino, Suppl. J. Phys. Soc. Jpn. **54** (1985) 321 (Proc. INS-RIKEN Int. Conf. on heavy ion physics, Mt. Fuji, 1984)
20) T. Kajino, H. Toki and S. Austin, preprint of Michigan State Univ. (1985), to be published
21) R.V. Wagoner, Astrophys. J. **178** (1973) 343;
Y. Yang *et al.*, Astrophys. J. **281** (1984) 493
22) S.M. Austin and C.H. King, Nature **269** (1977) 782;
S.M. Austin, Prog. Part. Nucl. Phys. **7** (1981) 1
23) G.M. Griffiths *et al.*, Canadian J. Phys. **39** (1961) 1397
24) M.J. Harris *et al.*, Ann. Rev. Astron. Astrophys. **21** (1983) 165;
W.A. Fowler, G.R. Caughlan and B.A. Zimmerman, Ann. Rev. Astron. Astrophys. **13** (1975) 69

25) J.A. Wheeler, Phys. Rev. **52** (1937) 1083 and 1107
26) M. Kamimura, Suppl. Prog. Theor. Phys. **62** (1977) 236
27) T. Ohmura *et al.*, Prog. Theor. Phys. **41** (1967) 391; **43** (1970) 347
28) A. Tohsaki, Suppl. Prog. Theor. Phys. **62** (1977) 191; Prog. Theor. Phys. **59** (1978) 1261
29) A.B. Volkov, Nucl. Phys. **74** (1965) 33
30) F. Tanabe, A. Tohsaki and R. Tamagaki, Prog. Theor. Phys. **53** (1975) 677
31) D.M. Brink and E. Boeker, Nucl. Phys. **A91** (1967) 1
32) K. Wildermuth and Y.C. Tang, A unified theory of the nucleus (Vieweg, Braunschweig, Germany, 1977)
33) H. Kanada, T. Kaneko and Y.C. Tang, Nucl. Phys. **A380** (1982) 87
34) K. Ikeda, H. Horiuchi and S. Saito, Suppl. Prog. Theor. Phys. **68** (1977)
35) T. Kajino, T. Matsuse and A. Arima, Nucl. Phys. **A413** (1984) 323; **A414** (1984) 185
36) T. Kajino, T. Matsuse and A. Arima, Proc. 10th Int. Conf. on few body problems in physics, Karlsruhe (1983), vol. II, 411
37) S.A. Moszkowski, in Alpha-, beta- and gamma-ray spectroscopy vol. 2, ed. by K. Siegbahn (North Holland, Amsterdam, 1966) p. 863
38) E.M. Burbidge *et al.*, Rev. Mod. Phys. **29** (1957) 547
39) A. Weller *et al.*, Phys. Rev. Lett. **55** (1985) 480
40) P.E. Cade and W.M. Huo, J. Chem. Phys. **47** (1967) 614
41) L. Wharton, L.P. Gold and W. Klemperer, Phys. Rev. **133B** (1963) 270;
S. Green, Phys. Rev. Abstracts 2, No. 10 (1971)
42) H. Orth, H. Ackermann and E.W. Otten, Z. Phys. **A273** (1975) 221
43) P. Egelhof *et al.*, Phys. Rev. Lett. **44** (1980) 1380
44) W.J. Vermmer *et al.*, Phys. Lett. **138B** (1984) 365; Australian J. Phys. **37** (1984) 273
45) P. Paul, J.B. Thomas and S.S. Hanna, Phys. Rev. **147** (1966) 774
46) D.St.P. Bunbury *et al.*, Proc. Phys. Soc. **A69** (1956) 165
47) D.M. Hardy *et al.*, Nucl. Phys. **A195** (1972) 250;
W.R. Boykin, S.D. Baker and D.M. Hardy, Nucl. Phys. **A195** (1972) 241;
R.J. Spiger and T.A. Tombrello, Phys. Rev. **163** (1967) 964
48) R. Tamagaki, Prog. Theor. Phys. **39** (1968) 91
49) F.C. Barker and R.H. Spear, Astrophys. J. **307** (1986) 847
50) R.D. Williams and S.E. Koonin, Phys. Rev. **C23** (1981) 2773
51) R.F. Christy and I. Duck, Nucl. Phys. **24** (1961) 89
52) A.R. Barnett *et al.*, Comput. Phys. Commun. **8** (1974) 377
53) A.F. Siegert, Phys. Rev. **52** (1937) 787
54) F.C. Barker, Nucl. Phys. **83** (1966) 418
55) S. Cohen and D. Kurath, Nucl. Phys. **73** (1965) 1 and **A101** (1967) 1
56) H.M. Hofmann and T. Mertelmeier, preprint
57) K. Langanke, preprint
58) L.R. Suelzle, M.R. Yearian and H. Crannell, Phys. Rev. **162** (1967) 992
59) G.J.C. van Niftrik *et al.*, Nucl. Phys. **A174** (1971) 173
60) F.A. Bumiller *et al.*, Phys. Rev. **C5** (1972) 391
61) O. Häusser *et al.*, Nucl. Phys. **A212** (1973) 613
62) J.H.E. Mattauch, W. Thiele and A.H. Wapstra, Nucl. Phys. **67** (1965) 1;
F. Ajzenberg-Selove, Nucl. Phys. **A320** (1979) 1; Atom. Nucl. Data Tables, **14** (1974) 485